

Metal-Azide-Pyrimidine Complexes $M(N_3)_2(pm)$ with a Three-Dimensional Network Showing Weak Ferromagnetism for M = Mn and Fe and Antiferromagnetism for M = Co and Ni

Yoshitaka Doi, Takayuki Ishida,* and Takashi Nogami*

Department of Applied Physics and Chemistry, The University of Electro-Communications, Chofu, Tokyo 182-8585

(Received June 7, 2002)

Antiferromagnetic phase transitions of $M(N_3)_2(pm)$ were observed at 51, 39, 41, and 46 K for M = Mn, Fe, Co, and Ni, respectively; here pm denotes pyrimidine. Single-crystal X-ray crystallographic analysis for M = Mn, Fe, and Co and powder X-ray diffraction measurements for M = Ni revealed that they were isomorphous. The N_3 and pm moieties contribute μ-1,3-bridged two-dimensional and μ-1,3-bridged one-dimensional structures, respectively, thus forming a three-dimensional framework. Antiferromagnetic couplings through the bridging ligands are consistent with superexchange mechanisms based on the coordination geometry determined. Small spin canting was observed below the transition temperature for M = Mn and Fe. The cant angles are estimated to be 0.06 and 0.13°, respectively, from the spontaneous magnetization at 10 K.

There have been numerous reports on infinite metal-organic polymeric frameworks involving N-donor bridging ligands.[1] We have reported the magnetism of pyrimidine(pm)-bridged transition metal complexes in connection with the high-spin *m*-phenylene-bridged poly-carbenes and -radicals.[2] The role of pm as magnetic couplers has been clarified to depend on the magnetic orbitals on the metal ions and the coordination geometries.[3] Various magnets have also been reported that contain d-transition metal ions and polycyano-anion bridges such as $N(CN)_2^-$.[4,5] Ternary systems are of increasing interest, and the peculiar crystal structures have been reported for $Mn[N(CN)_2]_2(pz)$[6] and $Cu[N(CN)_2]_2(pz)$,[7] where pz denotes pyrazine. We preliminarily reported the crystal structure and magnetic phase transition of $M^{II}[N(CN)_2]_2(pm)(solvent)$ (M = Fe,[8] Co,[8] Ni[9]) containing both $N(CN)_2^-$ and pm bridges. Their magnetic phase transition temperatures were generally low,[8,9] mainly because of the effective low dimensionality; the $N(CN)_2$ bridge works only as a μ-1,5-bridge that mediates much weaker magnetic exchange interaction than the μ-1,3-pm bridge. A copper(II) derivative $Cu[N(CN)_2]_2(pm)(CH_3CN)$ whose crystal structure was quite similar to those of $M[N(CN)_2]_2(pm)(solvent)$ (M = Fe, Co, Ni) was also synthesized, but it does not undergo any magnetic phase transition down to 2 K.[10] We turned our attention to shorter bridging anions. The azido-bridges are generally observed as end-on (μ-1,1) and end-to-end (μ-1,3) coordination modes, and their role as magnetic couplers have widely been investigated.[11,12] We prepared transition metal complexes, $M(N_3)_2(pm)$, with three-dimensional networks of transition metal ions containing both μ-1,3-azide and μ-1,3-pm bridges (the structural formula is shown in Chart 1; **1**, **2**, **3**, and **4** for M = Mn, Fe, Co, and Ni, respectively). We will describe here the crystal structures and magnetic properties of **1**–**4**. Escuer and co-workers have independently studied the crystal structure and magnetic property of **1**.[13] Our results on **1** are essentially the same as theirs. We will discuss here the comparison of the magnetic properties of **1** with those of **2**–**4**.

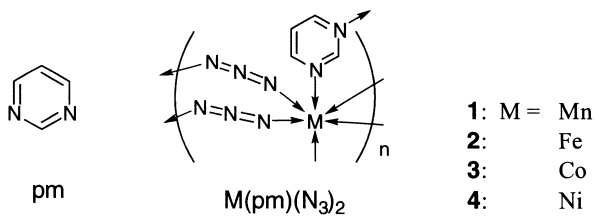

Chart 1.

Experimental

Caution. Azide derivatives are potentially explosive. Only a small amount of material should be prepared, and it should be handled with caution.

Materials. The following synthetic procedure is typical. An aqueous solution (1 cm^3) containing pm (79.9 mg, 1.00 mmol) and NaN_3 (130.2 mg, 2.00 mmol) was added to an aqueous solution (1 cm^3) of $MnCl_2{\cdot}4H_2O$ (198.5 mg, 1.00 mmol). The mixture was allowed to stand for several days to give colorless single crystals of $Mn(N_3)_2(pm)$ (**1**) suitable for X-ray diffraction study. Similar procedures using $FeCl_2{\cdot}4H_2O$ and $CoCl_2{\cdot}6H_2O$ in place of $MnCl_2{\cdot}4H_2O$ gave yellow and purple crystals of **2** and **3**, respectively. Preparation using $NiCl_2{\cdot}6H_2O$ gave light green fine powder of $Ni(N_3)_2(pm)$ (**4**). Elemental analyses (C, H, N) of **1**–**4** on a Fisons EA-1108 by a usual combustion method supported the formula of $M(N_3)_2(pm)$. Anal. Calcd. for $C_4H_4N_8Mn$ (**1**): C, 21.93; H, 1.84; N, 51.15%. Found: C, 21.53; H, 1.93; N, 50.56%. Calcd. for $C_4H_4N_8Fe$ (**2**): C, 21.84; H, 1.83; N, 50.94%. Found: C, 22.11; H, 1.67; N, 50.39%. Calcd. for $C_4H_4N_8Co$ (**3**): C, 21.54; H, 1.81; N, 50.23%. Found: C, 21.53; H, 1.78; N, 49.93%. Calcd. for $C_4H_4N_8Ni$ (**4**): C, 21.56; H, 1.81; N, 50.29%. Found: C, 21.52; H,

1.96; N, 49.92%.

X-ray Crystallographic Analysis. Diffraction data of single crystals of **1**–**3** were collected on a Rigaku R-axis RAPID diffractometer with graphite monochromated Mo $K\alpha$ radiation (λ = 0.71069 Å) at 90 or 100 K. The structures were directly solved by a heavy-atom Patterson method in the teXsan program package.[14] Numerical absorption correction was used. All of the hydrogen atoms could be found in difference Fourier maps, and the parameters of the hydrogen atoms were included in the refinement. The thermal displacement parameters were refined anisotropically for non-hydrogen atoms and isotropically for hydrogen atoms. Full-matrix least-squares methods were applied using all of the unique diffraction data. Crystallographic data have been deposited as Document No. 75044 at the Office of the Editor of Bull. Chem. Soc. Jpn. and also deposited with the CCDC (the reference numbers are 186730–186732 for **1**–**3**). Powder pattern data of **4** were recorded on a Rigaku RAD-B diffractometer with graphite monochromated Cu $K\alpha$ radiation (λ = 1.5418 Å) at 300 K. Refined cell constants were calculated on the Rietan2000 program[15] using all data in a range of $10° < 2\theta < 60°$.

Magnetic Measurements. Dc and ac magnetic susceptibilities of polycrystalline samples of **1**–**4** were measured on Quantum Design MPMS SQUID and PPMS magnetometers equipped with 7 and 9 T coils, respectively, in a temperature range down to 1.8 K. The magnetic responses were corrected with diamagnetic blank data of the sample holder obtained separately. The diamagnetic contribution of the sample itself was estimated from Pascal's constant. Ac magnetic susceptibilities were measured on a PPMS ac/dc magnetometer. An ac magnetic field (amplitude: 10 Oe, frequency: 100, 1000, and 10000 Hz) was applied to polycrystalline samples.

Results

X-ray Crystal Structure Analysis. Table 1 summarizes the X-ray crystallographic data for **1**–**3**. The crystals of **1**–**3** are practically identical, belonging to a space group monoclinic *C*2/*m*. Figure 1 shows the crystal structure of **2**. There is only one M ion in a crystallographically independent unit. Each octahedral M ion resides at an inversion center and is coordinated by four azide N atoms and two pm N atoms (Fig. 1(a)). The M ion and two N_3^- ions construct a two-dimensional network parallel to the *ac*-plane (Fig. 1(b)); an almost square lattice is formed by a repeating macrocyclic $[MN_3]_4$ motif. Selected bond lengths for **1**–**3** are listed in Table 2. In the coordination sphere of **1**–**3**, the bond length of M1–N1(pm nitrogen) is longer than those of other M1–N bonds, indicating that the pm nitrogen atoms are located at the axial positions. The pm molecules bridge inter-sheet M ions (Fig. 1(c)), and they construct a *trans* zigzag chain along the *b*-axis. In short, the N_3 and pm moieties contribute μ-1,3-bridged two-dimensional and μ-1,3-bridged one-dimensional structures, respectively, thus forming a three-dimensional framework. The pm plane is located in a nearly gauche manner with respect to the equatorial M–N bonds, as indicated by the dihedral angles of ca. 30° around C1–N1–M1–N2 (Table 2).

The intra-sheet M···M separations are 5.6–5.9 Å across the μ-1,3-azide bridges. The M···M separations of 6.0–6.1 Å across the pm bridge are slightly longer than those across the azide bridge. Since the $d_{x^2-y^2}$ and d_{z^2} are magnetic orbitals in high-spin manganese(II), iron(II), cobalt(II), and nickel(II) ions viewing from the electon configuration $(t_{2g})^n(e_g)^2$, both pm and azide bridges afford appreciable magnetic exchange pathways. The σ-type orbital overlap between the d_z^2 and nitrogen lone pair gives rise to antiferromagnetic superexchange coupling between two d_z^2 spins for pm-bridged complexes.[3] In the present complexes, the pm bridges can work as an antiferromagnetic coupler. Due to the strong directionality of the pm lone-pairs, the elongated octahedral axes of neighboring Mn ions are canted by 109.6(1)°. Within a two-dimensional Mn-azide network, the octahedral axes of neighboring Mn ions are also canted by the same angle. Similar structural arguments hold also for **2** and **3**.

Unfortunately, **4** was obtained only as a fine powder form. We measured the X-ray powder diffraction of **4**. The experimental and simulation results are summarized in Fig. 2. The

Table 1. Crystallographic Parameters of $M(N_3)_2(pm)$ (M = Mn, Fe, Co)

M	Mn	Fe	Co
Formula	$C_4H_4N_8Mn$	$C_4H_4N_8Fe$	$C_4H_4N_8Co$
Habit	Colorless needle	Orange needle	Pink needle
Crystal system	Monoclinic	Monoclinic	Monoclinic
Space group	*C*2/*m*	*C*2/*m*	*C*2/*m*
a / Å	11.325(2)	11.312(1)	11.197(1)
b / Å	12.278(3)	12.0984(8)	11.956(1)
c / Å	7.624(2)	7.5450(7)	7.5049(8)
β / °	129.88(1)	130.837(3)	130.645(3)
V / Å^3	813.5(3)	781.2(1)	762.3(2)
Z	4	4	4
d_{calc} / g cm^{-3}	1.789	1.870	1.943
T / K	90.	100.	100.
λ / Å	0.7107	0.7107	0.7107
μ / mm^{-1}	1.586	1.891	2.213
Reflections	888	901	902
$R(F^2)$ ($I > 2\sigma(I)$)	0.0469	0.0289	0.0324
$Rw(F)$ (all data)	0.1518	0.0880	0.0932
G.O.F.	1.333	1.117	1.499

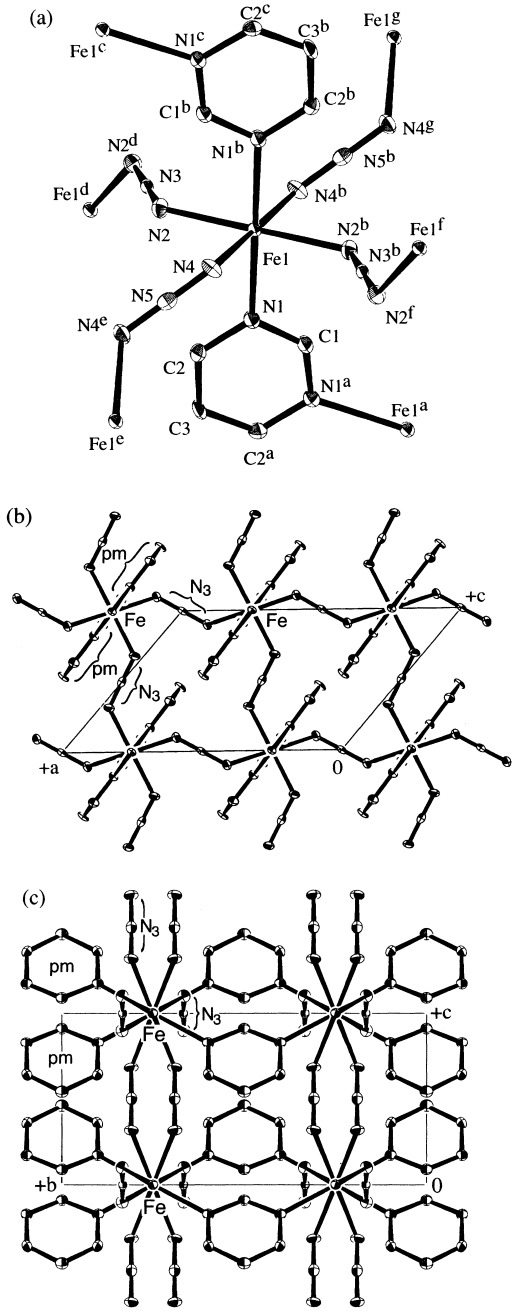

16

Fig. 1. Crystal structure of $Fe(N_3)_2(pm)$ (**2**). Hydrogen atoms are omitted for the sake of clarity. (a) Ortep drawing at the 50% probability level with atom labeling scheme. Symmetry codes: a: $x, -y, z$; b: $-x + 3/2, -y + 1/2, -z$; c: $-x + 3/2, y + 1/2, -z$; d: $-x + 1, y, -z$; e: $-x + 2, y, 1 - z$; f: $x + 1/2, -y + 1/2, z$; g: $x - 1/2, -y + 1/2, z - 1$. (b) Packing diagram viewed along the b axis. (c) Viewed along the a axis.

profile of **4** is consistent with the cell parameters of a = 11.07(1), b = 11.812(6), c = 7.40(1) Å, β = 130.42(6)°, and V = 737(1) Å^3, assuming a monoclinic $C2/m$ space group and Z = 4. These values are very close to those of **1**–**3** (Table 1). Since the simulation well reproduced the experimental profile, we can safely assume that the crystal structure of **4** is isostructural with those of **1**–**3**. From detailed comparison of the cell lengths and volume, an obvious trend of shrinkage of the cell can be found in the order of M = Mn, Fe, Co, and Ni. The covalent radii of metal ions are responsible for the shrinkage, as indicated by the difference of the M–N bond lengths (Table 2).

Table 2. Selected Bond Lengths, Angles, and Interatomic Distances of $M(N_3)_2(pm)$ (M = Mn, Fe, Co)[a)]

M	Mn	Fe	Co
M1–N1	2.283(3)	2.212(2)	2.165(2)
M1–N2	2.198(3)	2.153(2)	2.123(2)
M1–N4	2.219(3)	2.139(2)	2.125(2)
N1–M1–N2	90.1(1)	90.31(8)	90.56(6)
N1–M1–N4	91.4(1)	92.66(9)	92.60(7)
N2–M1–N4	92.7(1)	91.87(9)	92.05(7)
M1–N2–N3	124.0(2)	126.4(2)	125.6(1)
M1–N4–N5	124.2(2)	124.0(2)	124.1(1)
C1–N1–M1–N2	150.2(4)	149.7(3)	149.8(2)
C1–N1–M1–N4	−122.5(4)	−122.2(3)	−122.3(2)
M1···M1[a]	6.139(2)	6.0492(4)	5.9780(7)
M1···M1[d]	5.663(1)	5.6561(5)	5.5987(7)
M1···M1[e]	5.9010(1)	5.7539(1)	5.7385(1)

a) Symmetry codes: *a*: $x, -y, z$; *d*: $-x + 1, y, -z$; e: $-x + 2, y, 1-z$.

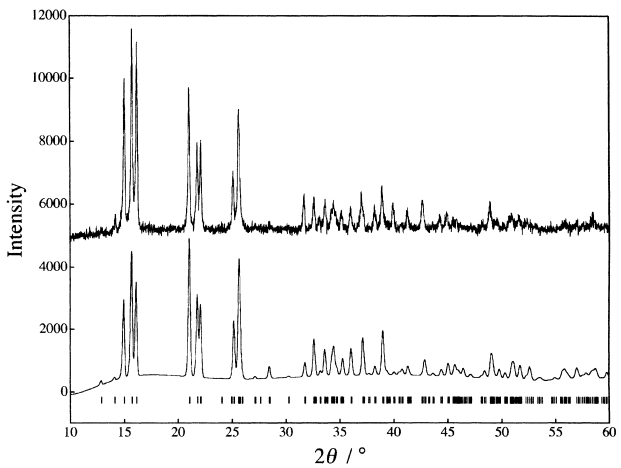

Fig. 2. Experimental (top) and simulated (bottom) profiles of powder X-ray diffraction pattern of $Ni(N_3)_2(pm)$ (**4**). Diffraction positions are indicated by ticks. Optimized cell parameters are: a = 11.07(1), b = 11.812(6), c = 7.40(1) Å, and β = 130.42(6)°.

Magnetic Properties. Figure 3 shows the temperature dependence of MT/H for **1**–**4** measured at 5 kOe. As a decrease of temperature, the MT/H value ($\chi_{mol}T$ value in a paramagnetic phase) decreased down to ca. 50 K in all cases, indicating the presence of dominant antiferromagnetic coupling among the metal spins.

A best fit of the magnetic susceptibility data of **1** above 200 K to the Curie–Weiss equation [$\chi_{mol} = C/(T - \theta)$] gave C =

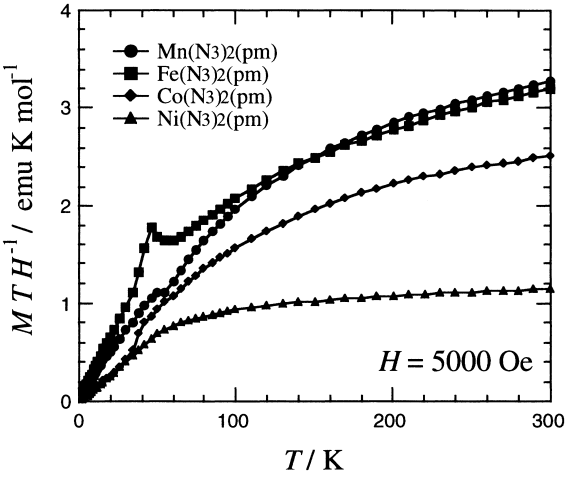

Fig. 3. Temperature dependence of *MT*/*H* for $M(N_3)_2(pm)$ (M = Mn, Fe, Co, and Ni) measured at 5 kOe.

4.56 cm^3 K mol^{-1} and $\theta = -119$ K for **1**. The Landé *g* factor of **1** was derived to be 2.04 for the above Curie constant (*C*) with $S = 5/2$. This g value is somewhat large but very close to that of isomeric $Mn(N_3)_2(pz)$ ($g = 2.03$).[16] The negative Weiss temperature (θ) value clearly indicates the presence of antiferromagnetic interaction among the Mn^{II} spins. A similar analysis for **2** gave $C = 4.62$ cm^3 K mol^{-1} and $\theta = -134$ K. The *g* factor was 2.48 with $S = 2$. The *MT*/*H* values of **1** and **2** do not show monotonic temperature dependence; there is a peak at about 45 K for **1** and a small dip is found at about 55 K for **2**. The size of these anomalies depended on the magnitude of the applied magnetic field. The field-cooled measurements at a small field will be described later.

On the other hand, the *MT*/*H* values of **3** and **4** exhibited monotonic temperature dependence. The Curie and Weiss constants obtained from the data above 200 K are: $C = 3.38$ cm^3 K mol^{-1} and $\theta = -104$ K for **3** and $C = 1.33$ cm^3 K mol^{-1} and $\theta = -49$ K for **4**. The *g* values of metal ions in **3** and **4** are 2.69 and 2.30, respectively. From a close look at the *MT*/*H* curve of **3**, a sharp drop can be found around 35 K, and the *M* vs *T* plot of **3** gave a sharp λ-type maximum at about 42 K (not shown). Similarly, the *M* vs *T* plot of **4** also shows a maximum at about 44 K. These findings suggest that the antiferromagnetic orderings take place around these temperatures.

We measured field-cooled magnetizations, remnant magnetizations, and zero-field-cooled magnetizations of **1**–**4**. The temperature dependence of the field-cooled magnetization at 5 Oe showed clear upsurges at about 51 and 40 K for **1** and **2**, respectively (Fig. 4(a)). After the applied field was removed, the remnant magnetizations disappeared at the same temperatures. The remnant magnetization was observed below the transition temperature in spite of the negative Weiss temperature, indicating that the specimen is a canted antiferromagnet (weak ferromagnet). To determine the magnetic phase transition temperatures more precisely, we performed ac magnetic susceptibility (χ_{ac}) measurements for **1**–**4**. As Fig. 4(b) shows, the real part of the ac magnetic susceptibility (χ_{ac}') exhibited

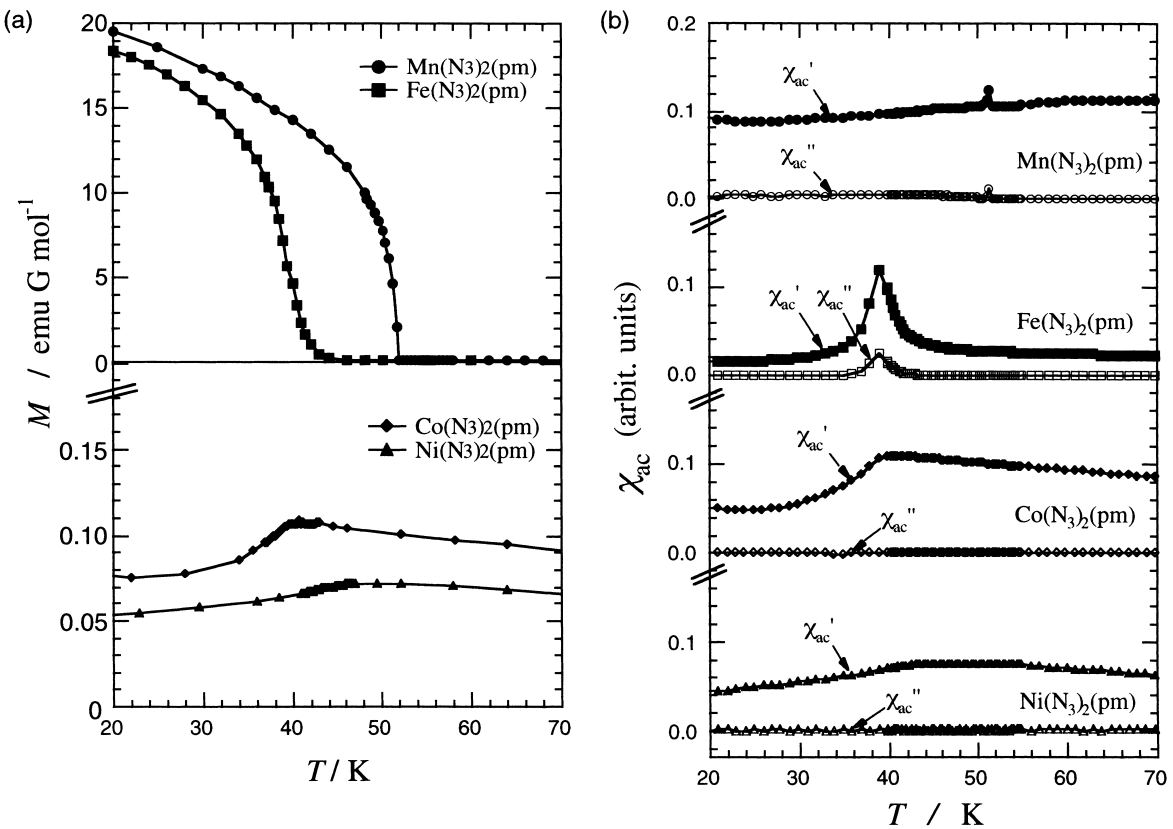

Fig. 4. (a) Field-cooled magnetization of $M(N_3)_2(pm)$ (M = Mn, Fe, Co, and Ni) measured at 5 Oe. (b) Ac susceptibility (χ_{ac}' and χ_{ac}'') of $M(N_3)_2(pm)$ (M = Mn, Fe, Co, and Ni) at an ac magnetic field of 10 Oe with a frequency of 1 kHz.

peaks at 51 and 39 K for **1** and **2**, respectively, supporting the occurrence of magnetic phase transition. Furthermore, the imaginary part of the ac susceptibility (χ_{ac}'') also showed peaks at the same temperatures. No frequency dependence was observed for ν = 100, 1000, and 10000 Hz, indicating that the materials have no spin-glass or superparamagnetic property. On the other hand, the χ_{ac}' of **3** shows an abrupt drop at 41 K on cooling, indicating that **3** is an antiferromagnet below 41 K. Similarly, the χ_{ac}' of **4** shows a decrease on cooling below 46 K. The rather broad peak seems to be caused by the poor crystallinity of **4** compared with those of **1**–**3**. The similarity of these magnetic properties of **3** and **4** is rationalized by taking the isomorphism into consideration. In sharp contrast to the case of **1** and **2**, the χ_{ac}'' of **3** and **4** exhibited no anomaly around the magnetic phase transition temperature, which suggests that the magnetic ground states of **1** and **2** are different from those of **3** and **4**.

In order to clarify the nature of magnetism below the transition temperature, we measured *M*–*H* curves for **1**–**4**. Figure 5(a) shows the magnetization curve of **1** measured at 10 K. The magnetization varied linearly up to 70 kOe, owing to strong antiferromagnetic interaction. This finding is compatible with the dominant antiferromagnetic behavior of **1** observed in the *MT*/*H* vs *T* plot (Fig. 3). However, we can find a small hysteresis loop in a low field region. The spontaneous magnetization extrapolated to $H \rightarrow 0$ Oe was found to be 30 erg Oe^{-1} mol^{-1} and the coercive field was 250 Oe (the inset of Fig. 5(a)). This magnetic behavior of **3** is typical of a weak ferromagnet (canted antiferromagnet). The cant angle was estimated to be 0.06° from $\sin^{-1}(M_{sp}/M_{sat})$ where M_{sp} and M_{sat} imply the spontaneous magnetization and saturation magnetization, respectively. A calculated M_{sat}, $N_A g \mu_B S$, was used in the above estimation because the magnetization did not saturate up to the highest applied field in our measurements.

Similarly, the *M*–*H* curve of **2** showed a basically antiferromagnetic nature with a hysteresis loop (Fig. 5(b)). The spontaneous magnetization was 60 erg Oe^{-1} mol^{-1} and the coercive force was 1200 Oe. The cant angle was estimated to be 0.13°.

On the other hand, the *M*–*H* curves of **3** and **4** indicate that they are genuine antiferromagnets. Figures 5(c) and 5(d) show that the magnetization varied almost linearly up to 90 kOe. In spite of the ambiguous broad peaks in the FCM and χ_{ac}' measurements of **4**, the *M*–*H* curve of **4** supports the occurrence of an antiferromagnetic phase transition. The curvature of the *M* vs. *H* plot (Fig. 5(d)) was convex downward on increasing an applied field, indicating a possible spin–flop transition on applying a further field. This curvature depends very little on temperature. Actually, the *M*–*H* curve of **4** measured at 2 K was essentially the same as that at 10 K; no obvious spin-flop transition was observed up to H = 90 kOe even at 2 K.

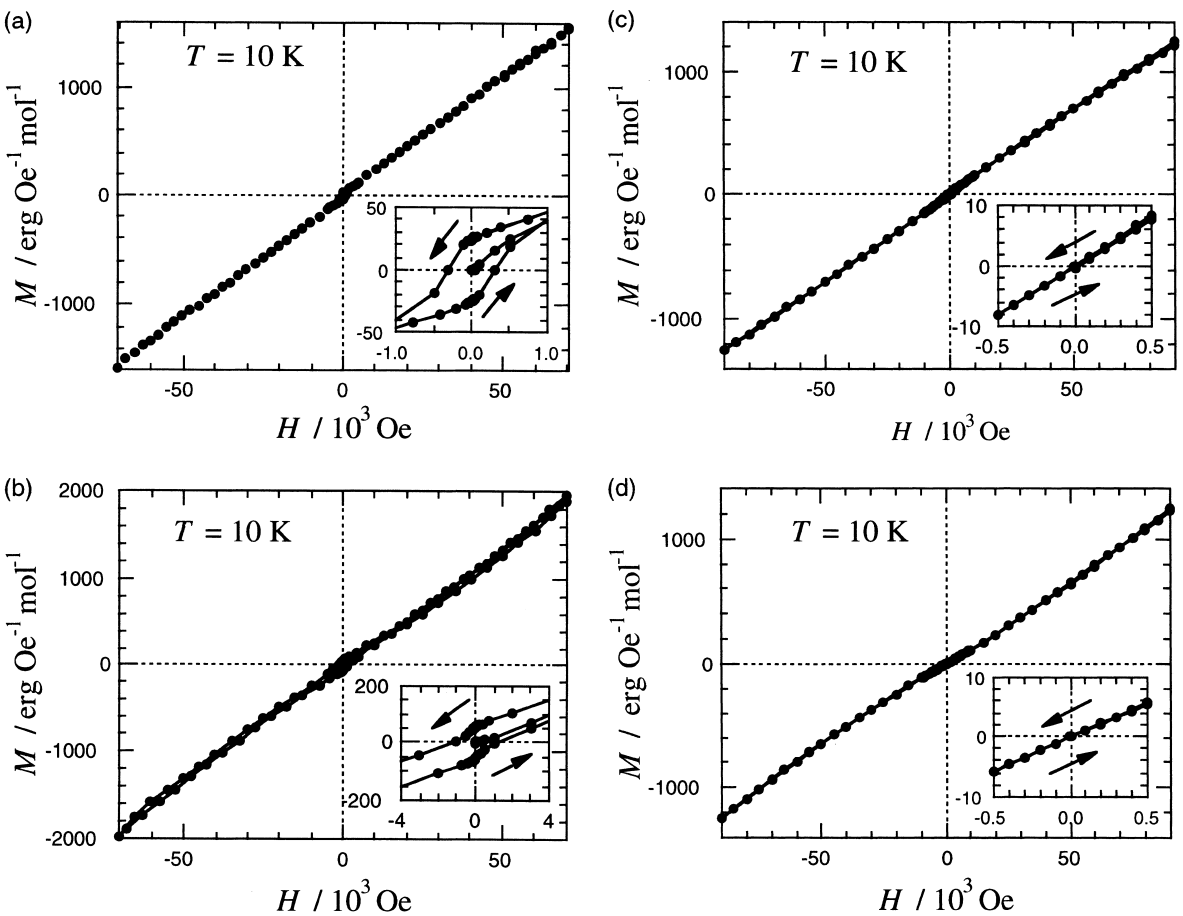

Fig. 5. *M*–*H* curves of $M(N_3)_2$(pm) (a, b, c, and d for M = Mn, Fe, Co, and Ni, respectively) measured at 10 K. Insets show a magnification of a low field region.

The downward curvature is responsible for the abrupt decrease in the *MT*/*H* vs *T* plot, which is characteristic of antiferromagnets. The canted antiferromagnets, **1** and **2**, exhibited a peak or dip of the *MT*/*H* values on cooling (Fig. 3), the origin of which is supposed as follows. The presence of spontaneous magnetization gives rise to an increase of the *MT*/*H* value while the downward curvature leads to a decrease of the *MT*/*H* values. The peak or dip is observed as a results of a balance of the two opposite effects. In fact, the anomalies of **1** and **2** in the *MT*/*H* vs *T* plot depend on the applied field as described above.

Discussion

The structural comparison between $M(N_3)_2(pm)$ and $M[N(CN)_2]_2(pm)$[8,9] indicates that the following features are common in spite of different crystal systems: 1) M^{II} and two anions construct a two-dimensional network. 2) Pm molecules bridge inter-sheet M^{II}, forming a pm-M *trans* zigzag chain. 3) Crystallographically asymmetric units contain only one metal ion. 4) Each octahedral M^{II} ion resides at an inversion center and is coordinated by four anion N atoms at the equatorial sites and by two pm N atoms at the axial sites. As Fig. 6 shows, similar networks of the crystal structures suggest that the mechanisms of canted antiferromagnetisms of $M(N_3)_2(pm)$ (M = Mn, Fe) and $M[N(CN)_2]_2(pm)$ (M = Fe, Co) are related to each other. Only the pm bridge in $M[N(CN)_2]_2(pm)$ brings about a main magnetic exchange pathway because the metal···metal distances across the $N(CN)_2$ bridge are rather long (ca. 9 Å).[8] On the other hand, both pm and N_3 bridges work as appreciable exchange couplers for $M(N_3)_2(pm)$ with the metal···metal distances of ca. 6 Å in three directions (Table 2). Namely, the latter has an ideal three-dimensional character but the former has a nearly one-dimensional character. A superexchange mechanism tells us that two d_z^2 spins should be antiferromagnetically correlated through the pm bridge.[3,8] The end-on-end azide bridges usually work as antiferromagnetic couplers.[11,12] Therefore, dominant antiferromagnetic orderings take place for both $M(N_3)_2(pm)$ and $M[N(CN)_2]_2(pm)$, but the transition temperatures are quite different (39 K vs 3.2 K[8] for M = Fe; 41 K vs 1.8 K[8] for M = Co; 46 K vs 8.3 K[9] for M = Ni). These findings can be regarded as a successful result in pursuing high-T_c (or T_N) materials by choosing smaller anions.

We demonstrated that **4** was an antiferromagnet, suggesting that the end-to-end N_3 bridge play the role of an antiferromagnetic coupler. Monfort and co-workers reported that a two-dimensional material containing nickel(II) and azide formed a ferromagnetic sheet, in which the end-to-end N_3 bridge works as a ferromagnetic coupler.[17] It has generally been found that end-to-end azide coordination gives rise to antiferromagnetic coupling whilst end-on coordination results in ferromagnetic coupling between nickel(II) and copper(II) ions.[11,12] Our result on **4** is normal and a possible reason for the difference of magnetic roles seems to originate from geometries such as torsion angles around M–N_3–M as well as bond angles around M–N–N. The crystal structure of **4** could not be determined and is only assumed to be isostructural with **1**–**3**. The following instance affords some valuable information. Do and co-workers reported ferromagnetic couplings in one-dimensional systems containing end-to-end azide-bridges.[18] The M–N_3–M torsion angles in their complex are 71.6 and 75.7° for M = Co and Ni, respectively. On the other hand, the Co–N_3–Co torsion angle of **3** was 108.5°, which does not lead to incidental orthogonality and consequently two cobalt ions are antiferromagnetically correlated. The Co–N–N bond angles for both complexes, which are another important geometrical parameter for magnetic coupling, fall into the usually observed range of 120–140°. Thus, the Co–N_3–Co torsion angle is more important for the magnetic coupling than the Co–N–N angles.

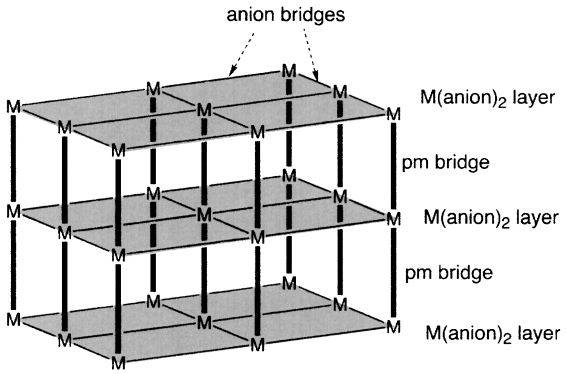

Fig. 6. Schematic drawing of the crystal structure of $M(X)_2(pm)$ (M = Mn^{2+}, Fe^{2+}, Co^{2+}, Ni^{2+}; X = N_3^-, $N(CN)_2^-$).

A canting angle for **1** of 0.06° was estimated from the small spontaneous magnetization (30 erg Oe^{-1} mol^{-1}). The canted antiferromagnetisms have often been found in three-dimensionally bridged transition-metal complexes, such as $M[N(CN)_2]_2$.[19] The Dzyaloshinsky–Moriya[20] mechanism was supposed for the canted antiferromagnetism of **1** in spite of the centrosymmetric crystal structure.[19] According to this interpretation, the small cant angle in **1** is reasonable because the cant angle is proportional to spin-orbit coupling, i.e., to the deviation of the g factor from 2.0023. The magnetic measurements revealed the *g* factor of **1** is 2.04. On the other hand, the cant angle of **2** is estimated to be 0.13°, which is considerably larger than that of the Mn complex. The large deviation of the *g* factor from 2.0023 was indicated by the observed *g* factor of 2.49, which is responsible for the large cant angle.

Cortés et al.[21] and Miller et al.[22] independently reported that the three-dimensional manganese(II) array of $Mn(N_3)_2$(4,4′-bipyridyl) showed weak ferromagnetism. The origin of the weak ferromagnetism was proposed to be due to the presence of an antisymmetric term in the Mn···Mn interaction in spite of *g* equaling 2.00 because it crystallized in an acentric space group.[22] However, there is an only one metal ion in a crystallographically independent unit of $M(N_3)_2(pm)$ and the crystal inversion center resides at the metal ion site. A possible explanation for the antisymmetric exchange mechanism is a structural modulation which leads to a lower crystal symmetry involving slightly different metal sites.

The weak-ferromagnetic behavior is intrinsic and reproducible, as supported by the parallel work on **1** done by Escuer et al.[13] They also found a weak-ferromagnetic ordering below 50 K and a very weak (0.003 $N_A\mu_B$) remnant magnetization at 2 K. Although the *M*–*H* curve was not shown,[13] this remnant value is supposed to be consistent with M_{sp} in the present study, because the estimation of M_{sp} by extrapolation is usually

larger than the observed remnant magnetization. They suggested that the spin canting originated from the large dihedral angle between the Mn-azide planes of neighbouring units. We have to add a comment on the geometry of the inter-plane Mn–pm–Mn zig-zag array. The large dihedral angles are found at neighboring units in all three directions, and all of the Mn···Mn distances are comparable due to μ-1,3-bridges in every neighboring unit. Therefore, the spin canting may originate from the large dihedral angles across the pm bridges as well as across the azide bridges.

Although the crystal structures of the present series are isomorphous, **1** and **2** are canted antiferromagnets but **3** and **4** are antiferromagnets. Unexpectedly, **1** containing manganese(II) ions is a canted antiferromagnet whereas **3** containing cobalt(II) ions is an antiferromagnet. The cobalt(II) ion usually has a large single-ion magnetic anisotropy and a large deviation of g from 2.0023, which might favor canted magnetic structures. Actually, the series of $M^{II}[N(CN)_2]_2(pm)$ (M = Fe, Co, Ni) were characterized as canted antiferromagnets.[8,9] In the series of $MCl_2(pm)_2$, the iron(II) and cobalt(II) derivatives were canted antiferromagnets[23] but the nickel(II) one was a normal antiferromagnet.[24] The present result indicates that various magnetic ground states are influenced not only by single ion anisotropy. Detailed structural differences of the coordination structure and the magnetic orbitals among the electron configurations of d^5, d^6, d^7, and d^8 should also be taken into account together with the crystal structure modulation as described above. More curious results were reported for the $M[N(CN)_2]_2$ series: canted antiferromagnets were obtained for M = Mn and Fe, but ferromagnetic orderings were observed for M = Co and Ni.[5] The origin of these various magnetic behaviors has not been clarified sufficiently and further investigation is required.

In summary, the basically antiferromagnetic structures were characterized for all of the complexes investigated here, being consistent with dominant antiferromagnetic couplings both across the pm and azide bridges. The presence or absence of spin canting is found to depend on the metal ion species; the manganese(II) and iron(II) derivatives are weak ferromagnets and the cobalt(II) and nickel(II) ones are antiferromagnets.

We acknowledge Dr. Masanori Yasui and Prof. Fujiko Iwasaki, The University of Electro-Communications, for their kind assistance in the X-ray powder diffraction analysis. This work was supported by a Grant-in-Aid for Scientific Research on Priority Areas of "Molecular Conductors and Magnets" (No. 730/11224204) and by a Grant-in-Aid for Scientific Research (No. 13640575), both from the Ministry of Education, Culture, Sports, Science and Technology.

References

1 P. J. Stang and B. Olenyuk, *Acc. Chem. Res.*, **30**, 502 (1997); O. M. Yaghi, H. Li, C. Davis, D. Richardson, and T. L. Groy, *Acc. Chem. Res.*, **31**, 474 (1998); M. Eddaoudi, D. B. Moler, H. Li, B. Chem, T. M. Reineke, M. O'Keeffe, and O. M. Yaghi, *Acc. Chem. Res.*, **34**, 319 (2001); S. Kitagawa and M. Kondo, *Bull. Chem. Soc. Jpn.*, **71**, 1739 (1998).

2 T. Ishida and T. Nogami, *Recent Res. Devel. Pure Appl. Chem.*, **1**, 1 (1997).

3 T. Ishida, S.-i. Mitsubori, T. Nogami, N. Takeda, M. Ishikawa, and H. Iwamura, *Inorg. Chem.*, **40**, 7059 (2001); T. Ishida, T. Kawakami, S.-i. Mitsubori, T. Nogami, K. Yamaguchi, and H. Iwamura, *J. Chem. Soc., Dalton Trans.*, **2002**, 3177.

4 S. R. Batten, P. Jensen, B. Moubaraki, K. S. Murray, and R. Robson, *Chem. Commun.*, **1998**, 439; M. Kurmoo and C. J. Kepert, *New J. Chem.*, **22**, 1515 (1998); J. L. Manson, C. R. Kmety, Q. Z. Huang, J. W. Lynn, G. M. Bendele, S. Pagola, P. W. Stephens, L. M. Liable-Sands, A. L. Rheingold, A. J. Epstein, and J. S. Miller, *Chem. Mater.*, **10**, 2552 (1998); J. L. Manson, C. R. Kmety, A. J. Epstein, and J. S. Miller, *Inorg. Chem.*, **38**, 2552 (1999).

5 J. S. Miller and J. L. Manson, *Acc. Chem. Res.*, **34**, 563 (2001).

6 J. L. Manson, C. D. Incarvito, A. L. Rheingold, and J. S. Miller, *J. Chem. Soc., Dalton Trans.*, **1998**, 3705; J. L. Manson, Q.-z. Huang, J. W. Lynn, H.-J. Koo, M.-H. Whangbo, R. Bateman, T. Otsuka, N. Wada, D. N. Argyriou, and J. S. Miller, *J. Am. Chem. Soc.*, **123**, 162 (2001).

7 P. Jensen, S. R. Batten, G. R. Fallon, D. C. R. Hockless, B. Moubaraki, K. S. Murray, and R. Robson, *J. Solid State Chem.*, **145**, 387 (1999).

8 T. Kusaka, T. Ishida, D. Hashizume, F. Iwasaki, and T. Nogami, *Chem. Lett.*, **2000**, 1146; T. Kusaka, T. Ishida, and T. Nogami, *Mol. Cryst. Liq. Cryst.*, **379**, 259 (2002).

9 T. Kusaka, T. Ishida, D. Hashizume, F. Iwasaki, and T. Nogami, *Mol. Cryst. Liq. Cryst.*, **376**, 463 (2002).

10 I. Riggio, G. A. van Albada, D. D. Ellis, A. L. Spek, J. Reedijk, *Inorg. Chim. Acta*, **313**, 120 (2001).

11 E. Ruiz, J. Cano, S. Alvarez, and P. Alemany, *J. Am. Chem. Soc.*, **120**, 11122 (1998); P. Chaudhuri, T. Weyhermüller, E. Bill, and K. Wieghardt, *Inorg. Chim. Acta*, **252**, 195 (1996).

12 O. Kahn, "Molecular Magnetism", VCH, New York (1993), Chap. 6.

13 A. Escuer, R. Vicente, F. A. Mautner, M. A. S. Goher, and M. A. M. Abu-Youssef, *Chem. Commun.*, **2002**, 64.

14 "teXsan: crystal structure analysis package," Molecular Structure Corp., The Woodlands, TX (1985, 1999).

15 "Rietan2000": F. Izumi and T. Ikeda, *Mater. Sci. Forum*, **321-324**, 198 (2000).

16 J. L. Manson, A. M. Arif, and J. S. Miller, *Chem. Commun.*, **1999**, 1479.

17 M. Monfort, I. Resino, J. Ribas, and H. Stoeckli-Evans, *Angew. Chem., Int. Ed. Engl.*, **39**, 191 (2000).

18 C. S. Hong, J.-e. Koo, S.-K. Son, Y. S. Lee, Y.-S. Kim, and Y. Do, *Chem. Eur. J.*, **7**, 4243 (2001).

19 S. R. Batten, P. Jensen, C. J. Kepert, M. Kurmoo, B. Moubaraki, K. S. Murray, and D. J. Price, *J. Chem. Soc., Dalton Trans.*, **1999**, 2987.

20 I. Dzyaloshinsky, *J. Phys. Chem. Solids*, **4**, 241 (1958); T. Moriya, *Phys. Rev.*, **120**, 91 (1960).

21 S. Martín, M. G. Barandika, L. Lezama, J. L. Pizarro, Z. E. Serna, J. I. R. de Larramendi, M. I. Arriortua, T. Rojo, and R. Cortés, *Inorg. Chem.*, **40**, 4209 (2001).

22 S. Han, J. L. Manson, J. Kim, and J. S. Miller, *Inorg. Chem.*, **39**, 4182 (2000).

23 K. Nakayama, T. Ishida, R. Takayama, D. Hashizume, M. Yasui, F. Iwasaki, and T. Nogami, *Chem. Lett.*, **1998**, 497.

24 K. Zusai, T. Kusaka, T. Ishida, R. Feyerherm, M. Steiner, and T. Nogami, *Mol. Cryst. Liq. Cryst.*, **343**, 127 (2000).